CCFE-PR(17)58

I. Waters, S. Silburn, H. Frerichs, Y. Feng, J. Harrison, A. Kirk,
and O. Schmitz

Field Aligned Flows Driven by Neutral Puffing at MAST

Field Aligned Flows Driven by Neutral Puffing at MAST

I. Waters,[1] S. Silburn,[2] H. Frerichs,[1] Y. Feng,[3] J. Harrison,[2] A. Kirk,[2] and O. Schmitz[1]

[1]University of Wisconsin-Madison, Madison, Wisconsin, USA
[2]Culham Centre for Fusion Energy, Abingdon, Oxfordshire, United Kingdom
[3]Max-Planck-Institut für Plasmaphysik, Greifswald, Germany

Field Aligned Flows Driven by Neutral Puffing at MAST

I. Waters,[1, a)] S. Silburn,[2] H. Frerichs,[1] Y. Feng,[3] J. Harrison,[2] A. Kirk,[2] and O. Schmitz[1]
[1)] *University of Wisconsin-Madison, Madison, Wisconsin, USA*
[2)] *Culham Centre for Fusion Energy, Abingdon, Oxfordshire, United Kingdom*
[3)] *Max-Planck-Institut für Plasmaphysik, Greifswald, Germany*

(Dated: 12 September 2017)

Methods for density control are of critical importance for future long pulse tokamaks. The EMC3-EIRENE code is being used to investigate the applicability of 3D non-axisymmetric fields for density control in standard and advanced divertor configurations in spherical tokamaks. Part of this effort is understanding Scrape Off Layer (SOL) transport mechanisms once axisymmetry is broken. Unique experimental measurements of SOL flow structures at the Mega Ampere Spherical Tokamak (MAST) present an ideal laboratory for comparison between experiment and modeling. A Coherence Imaging Spectroscopy (CIS) diagnostic was deployed for the MAST 2013 scientific campaign, during which flow measurements were taken of high field side fueling experiments that show the appearance of field-aligned flows around the center column. EMC3-EIRENE simulations are in good agreement with these measurements, and in tandem with 1D analysis show that the code captures the fundamental dynamics underlying the observed behavior. Neutral fueling of a flux tube creates a local plasma source, this drives a local increase in static plasma pressure, which in turn leads to a flow away from the particle source in that flux tube. Cross field diffusion then damps these parallel flows.

PACS numbers: 52.25.Fi, 52.25.Jm, 52.30.Cv, 52.55.Fa, 52.65.Kj, 52.65.Pp, 52.70.Kz

I. INTRODUCTION

Methods for density control are of critical importance for future long pulse tokamaks. This is complicated by proposed solutions to damaging transient heat loads such as 3D magnetic perturbations[1–3]. These changes to the magnetic fields will induce flows in the Scrape-Off-Layer (SOL), and change plasma conditions in regions important for neutral fueling[4]. The EMC3-EIRENE code (Section II B) is being used to investigate the impact of these 3D non-axisymmetric fields for density control in standard and advanced divertor configurations in spherical tokamaks. It is necessary to understand SOL transport mechanisms once the axisymmetry in a system is broken, and modeling can enable the identification of the core physical mechanisms at work.

Additionally, due to the prominence of the Plasma-Material Interaction challenge in future tokamaks, current experimental facilities are increasingly focusing on new diagnostics and methods of measuring important plasma parameters in the SOL and divertor regions. The Mega Ampere Spherical Tokamak and its forthcoming Upgrade (MAST and MAST-U respectively) have a particular focus on novel divertor scenarios and exhaust physics. As a result, MAST and MAST-U are a natural fit for these larger EMC3-EIRENE studies. In particular, unique experimental measurements of SOL flow structures at MAST are an ideal laboratory for comparison.

[a)] iwaters@wisc.edu; 3dpsi.engr.wisc.edu

II. METHODS

A. Coherence Imaging Spectroscopy

A Coherence Imaging Spectroscopy (CIS) diagnostic was deployed for the MAST 2013 scientific campaign to measure impurity ion flows in the SOL and divertor[5]. CIS is based on narrow-band imaging Fourier transform spectroscopy, which can provide time-resolved 2D imaging of emission line brightness, width and center wavelength over wide fields of view[6,7]. Flows are measured using CIS by measuring the Doppler shift of impurity ion emission lines. The large amount of spatial information provided by this technique makes it ideal for studying localized and dynamic phenomena in the plasma edge. During the 2013 MAST campaign the CIS instrument was used to study flows in both the main chamber SOL and divertor, using C^+ (514.2 nm), C^{2+} (464.8 nm), and He^+ (468.6 nm) spectral lines. By imaging in the different impurity lines, flow structures in different depths of the SOL can be accessed, based on which lines local plasma temperatures were exciting: flows deeper in the plasma could be imaged in He^+ whereas in the outer SOL C^+ was most emissive.

When observing C^{2+} flows at the high field side (HFS) SOL near the midplane, a particularly striking observation was the formation of field-aligned flow structures under certain conditions, with neighboring flux tubes showing flow in opposite directions around the center column. Specifically, when Deuterium gas fueling from a valve at the inboard midplane was used and the distance from the gas valve to the plasma separatrix according to EFIT was sufficiently small (< 2.5cm), such patterns were robustly observed to form, with such data obtained in 45 pulses. An example of an image from the CIS instrument of such

flows is shown in Figure 1. Parallel flow velocities estimated from this data are typically in the range 5 - 25 km/s.

B. EMC3-EIRENE Modeling

The EMC3-EIRENE code was then deployed to better understand these novel measurements of high field side structures. EMC3-EIRENE is a fluid edge plasma code coupled to EIRENE–a kinetic transport code for neutrals. While originally designed for inherently 3D magnetic systems (e.g. stellarators[8]), EMC3-EIRENE has also been used for 3D perturbations to largely axisymmetric systems (e.g. tokamaks with applied resonant magnetic fields[9–11]), and–of particular interest for this work–has the capability to include non-axisymmetric fueling sources. With work towards increasing complexity with respect to the 3D nature of plasma devices–like fueling[12], impurity seeding[13], and even localized heating by ECRH[12]–in EMC3-EIRENE simulations, it is important to validate that the code captures the core physics that drive SOL exhaust.

A series of simulations was carried out that included the full toroidal and poloidal extent of the MAST edge plasma. Neutral particles were then thermally sourced from a single location on the center column. Additional fueling via neutral recycling from plasma facing components was then self consistently adjusted to maintain a constant user defined density at the inner surface boundary of the modeling domain. Power and inner simulation boundary density were held fixed while neutral puffing rates, and cross-field terms were varied. Unless otherwise noted simulations were carried out without parallel viscosity terms. These simulations showed good qualitative agreement with experiment in that the same field-aligned flows were observed around the center column when HFS neutral fueling was included as shown in Figure 1.

Important plasma parameters such as flow, temperature, plasma density, and plasma source density can be extracted along an entire field line to get a better picture of steady state plasma behavior in the parallel direction. Irrespective of the neutral puffing input rate, similar features are seen in the evolution of the flow in the flux tube. All fueling cases are characterized by a highly localized plasma source, and–as shown in Figure 2–a rapid increase in parallel flow away from the source location in both directions along the field line. This is followed by a more gradual decay of flow further along the field line. The ionization of neutrals results in a local drop in plasma temperature and an increase in density which results in static plasma pressure ($p = n * (kT_e + kT_i)$) increasing dramatically (Figure 2.a) in the region of the neutral puff, resulting in pressure driven flows along the field lines (Figure 2.b).

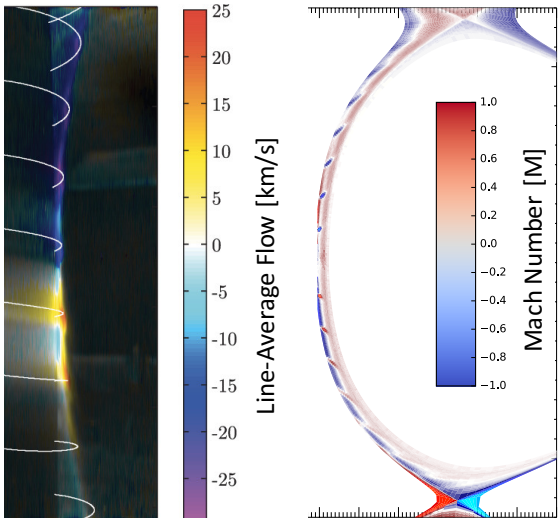

FIG. 1: Image from CIS diagnostic showing field aligned structures in CIII+ with color showing the measured velocity (left) with EMC3-EIRENE simulation showing qualitatively similar field aligned flows in the bulk plasma (right).

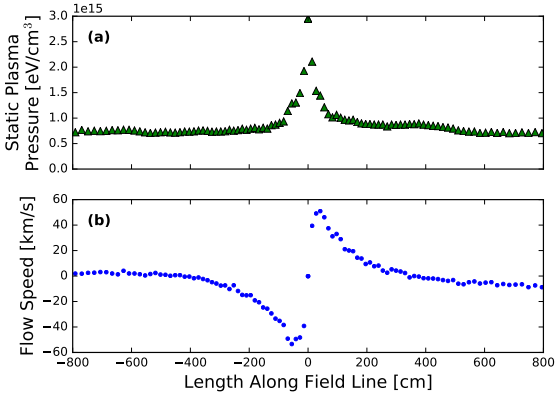

FIG. 2: Static plasma pressure (a) and parallel plasma flow (b) along a field line launched from immediately in front of neutral puffing site (Z = 0.0 cm, ϕ=0.0, R = 19.6 cm). Highly localized plasma pressure spike drives plasma flow away from neutral puff.

C. 1-D Models

To better understand the features of the EMC3-EIRENE results, comparative modeling was carried out using a 1D isothermal fluid model (see[4] Chapter 10.2). However, to more clearly understand the behavior of the underlying functions, we move into a unit less formulation of the functions for density ($n(x)$) and velocity ($u(x)$):

$$\rho(\xi) = \frac{n(x)}{n_{bg}}, M(\xi) = \frac{u(x)}{c_s} \quad (1)$$

And introduce the modeling parameter:

$$\alpha_S = \frac{S_0}{n_{bg} c_s} \tag{2}$$

Where we define n_{bg} as some prescribed background density, c_s as the sound speed, L as a perturbation scale length, ξ as a unit less length parameter equal to x/L, and S_0 as the source strength of a Gaussian function.

The isothermal model can then be expressed as a coupled pair of Particle (Eq. 3) and momentum (Eq. 4) conservation equations in an infinite flux tube:

$$\frac{d}{d\xi}(\rho M) = \alpha_S \frac{e^{\frac{-\xi^2}{2}}}{\sqrt{2\pi}} \tag{3}$$

$$\frac{d}{d\xi}(\rho M^2 + \rho) = 0 \tag{4}$$

In this ideal model, a localized particle source leads to pressure driven flows that stabilize and remain constant in these infinite flux tube conditions. It is interesting to note that in this unit less formulation, in a diffusion-less flux tube the value of $\rho(\xi = 0)$ must be greater than the source parameter α_S or the flow solution will reach an unphysical singularity where $M = 1$. This is a reflection of no *steady state* solution existing for this scenario in an isothermal plasma[4].

This is not what we see in the EMC3-EIRENE simulations when looking along a single field line. To better understand this behavior in the more complex simulation, complexity is added back into the 1D model with the addition of cross field terms. The ansatz is made that the perturbed field line, where a plasma source is being added, interacts with a background field line with zero flow and a fixed density. The perturbed field line then loses momentum and particles at some rate $D_\perp$, over some scale length δ, and is proportional to the difference between the quantity (density or flow) on the two field lines. We can then define a diffusion parameter for our unit less equations:

$$\alpha_D = \frac{D_\perp L}{\delta^2 c_s} \tag{5}$$

Which we then introduce back into new particle (6) and momentum (7) conservation equations:

$$\frac{d}{d\xi}(\rho M) = \alpha_S \frac{e^{\frac{-\xi^2}{2}}}{\sqrt{2\pi}} + \alpha_D(1 - \rho) \tag{6}$$

$$\frac{d}{d\xi}(\rho M^2 + \rho) = -\alpha_D \rho M \tag{7}$$

These equations can then be solved by setting input parameters of α_D and α_S, and treating the equation as a boundary value problem. At some distance from the stagnation point (many times the length scale of the perturbation, e.g. $\xi = 50$), it is assumed that the density parameter $\rho(\xi)$ is equal to or very close to one (i.e. that the density returns to the background value at some very large distance from the perturbation). Then, we apply the ansatz that the flow speed $M(\xi) = 0$ at the stagnation point ($\xi = 0$) goes to zero. With these boundary conditions numerical methods can be used to find self consistent steady state solutions for $\rho(\xi)$ and $M(\xi)$ that are symmetric about the location of puffing.

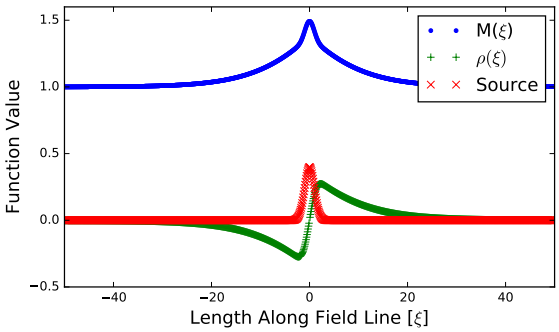

FIG. 3: Solving Eqs. 6 and 7 self consistently while imposing initial conditions on ρ at $\xi = 50$ and on M at $\xi = 0$ in an infinite flux tube. Shows good qualitative agreement with EMC3-EIRENE results in Figure 2.

Figure 3 shows the results of this process for $\alpha_S = 1$ and $\alpha_D = \frac{1}{5}$ (i.e. $kT = 25$ eV, $L = 1$ cm, $D_\perp = 1$ cm^2/s, and $\delta = 1$ cm) using the shooting method and an initial value of $\rho(\xi = 50) = 1.0$. The flow locally peaks, and then exponentially decays along the field line until reaching the equilibrium values.

III. RESULTS

A. Impacts of Different Neutral Puffing Rates

To further investigate the 3D edge, it is useful to look not only along a single field line as in Fig. 2, but along a set of neighboring field lines to build a ribbon of plasma information. This 'flux ribbon' provides a cross section of the behavior in the flux tube from the area immediately in front of the neutral puffing location, to areas deeper into the plasma. By launching field lines from sufficiently close positions (1 mm from point to point) and constraining our investigation to within 4 meters of the neutral puffing along a field line, geometric impacts of flux expansion can be ignored.

Figure 4 shows a series of these flux ribbons for 4 different fueling scenarios, from no neutral puffing, to a puffing rate of 6.2×10^{20} neutrals per second from a single point. The figure shows bulk plasma flow in normalized Mach units. The intense localized plasma source caused by the neutral puffing drives strong flows. However, the peak flow location and overall structure of the flows isn't

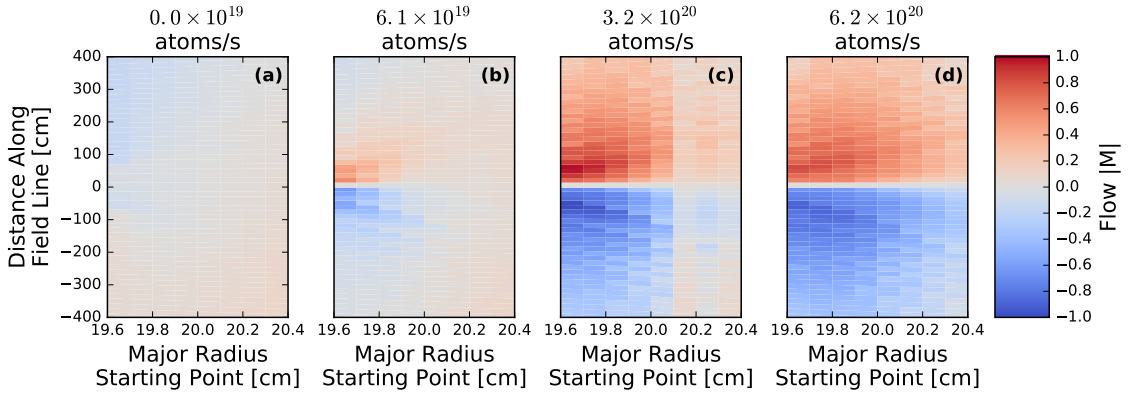

FIG. 4: Flow for 4 fueling scenarios in EMC3-EIRENE simulations ((a) = no neutral fueling, $(b) = 6.2 \times 10^{19}$ atom/s, $(c) = 3.1 \times 10^{20}$ atom/s, $(d) = 6.2 \times 10^{20}$ atom/s). Increased fueling drives increasingly strong parallel flows.

impacted by the puffing rate. Additional neutrals being introduced into the plasma only change the overall magnitude of the flows.

B. Cross Field Diffusion Driven Flow Decay

Simulations were also carried out in EMC3-EIRENE with different cross field diffusion rates ($D_\perp[m^2/s] = 0.1$, 0.3, and 1.0, and $\chi_\perp = 3D_\perp$), but with fueling and inner simulation densities kept constant. Field line profiles (starting at the point Y = 0.0 cm, Z = 0.0 cm, R = 19.9 cm, i.e. 3 mm in front of the puffing location and the middle column of data in Figure 4) of flow are shown for the three diffusion values in Figure 5. It can be seen that in the major toroidal direction, the high diffusion coefficient case decays to 20 km/s almost 50% sooner than the lowest diffusion coefficient. In general, the equilibrium (and thus the EMC3-EIRENE simulation) does not have up-down symmetry. Thus, the field line is encountering different plasma parameters in the one direction (up the center column) versus the other direction (down the center column) and this difference in the background plasma may be responsible for observed asymmetries.

Figure 5 also shows a case where the parallel viscosity term in the EMC3-EIRENE equations–typically omitted–is re-introduced into the simulation for the $D_\perp = 0.3$ m^2/s case. We retain the same qualitative result for the flow with parallel viscosity included. However, the addition of this viscosity term does lead to a decrease in the peak flow reached, and causes this peak to be obtained further along the field line. The addition of parallel viscous terms acts to retard the parallel escape of particles along a field line, thus static plasma pressure in the region of the source is enhanced by a factor of two. This increase in local pressure also results in a further perpendicular extension of the region of high pressure as shown in Figure 6. It can also be seen that with parallel viscous terms acting on the plasma that the region of peak static pressure is no longer immediately in front of the neutral puff, but 2-3 mm into the plasma. The energy loss due to ionizations drives the plasma temperature immediately in front of the puffing location down, which more than balances out the increase in plasma density. Only further into the plasma does the balance of particle sources *and* energy sources provide the maximum pressure.

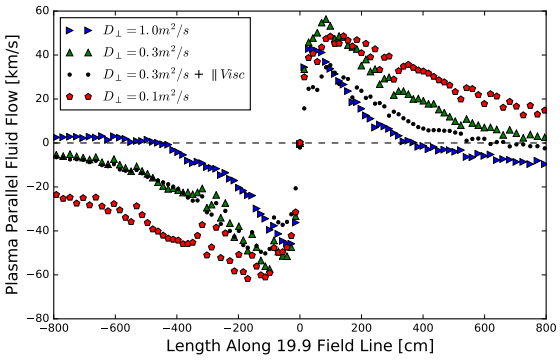

FIG. 5: Extracted profiles along the same field line in simulations with 3 different perpendicular diffusion constants ($D_\perp = 0.3$ m^2/s with and w/o $\|$-viscosity) showing that low diffusion leads to longer lived flows.

IV. DISCUSSION

The insights gained from detailed analysis of the modeled results–namely the characteristic decay of the flow along a field line–motivates further analysis of experimental results. Since the CIS diagnostic measures emission line Doppler shift, the measurement gives the flow velocity component towards or away from the camera, and line-integrated along the diagnostic line-of-sight weighted by the local emission intensity. An estimate of the parallel flow speed can be extracted using the EFIT equilibrium and knowledge of the diagnostic viewing geom-

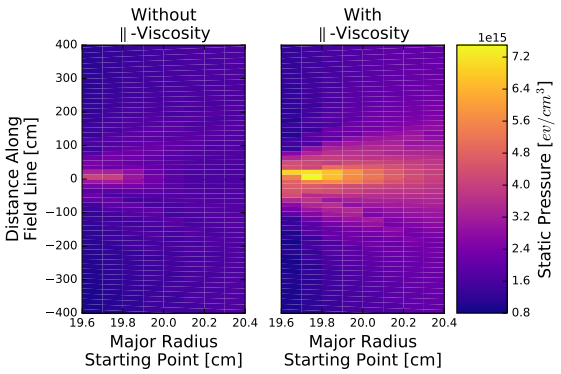

FIG. 6: Static plasma pressure along and across the effective flux tube in a $D_\perp = 0.3$ m^2/s plasma without (left) and with (right) parallel viscous forces included in the simulation.

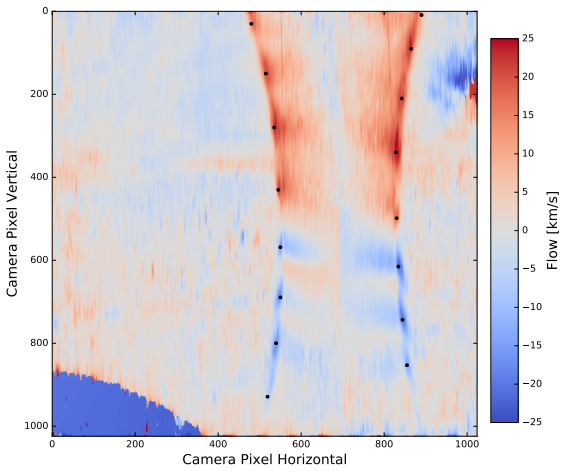

FIG. 7: Image from post processed CIS diagnostic showing flow speed in km/s and with points indicating sampling locations for data in Figure 8.

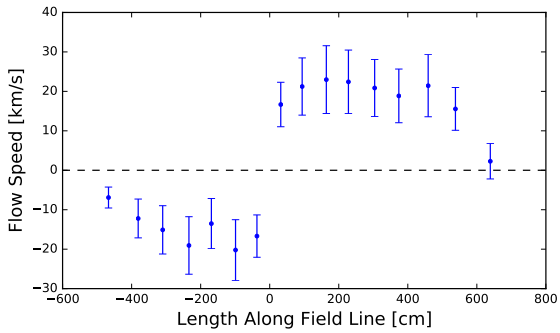

FIG. 8: The measured CII+ velocity along a field line measured at the points shown in Figure 7. Qualitatively shows good agreement with the lowest diffusion coefficient in Figure 5, $D_\perp = 0.1$ m^2/s.

etry. First, the sight-line vectors corresponding to each diagnostic pixel are obtained using the CalCam code[14], which allows spatial calibration of the camera by matching features in images of the MAST vessel with features in a corresponding CAD model. Since the impurity line emission appears in a narrow shell in the scrape-off-layer, and due to the camera viewing geometry, the largest contribution to the diagnostic signal, and therefore the best localization of the flow measurement, is localized close to a curved plane where the camera sight-lines are tangent to the toroidal direction, known as the tangency plane. It is assumed that the measured velocity is entirely in the parallel direction with respect to the magnetic field and that cross field diffusion speeds are minimal. Then, the parallel flow at each point in the tangency plane can then be estimated as $v_{||} \approx v_{measured}/\mathbf{B}\cdot\mathbf{L}$, where $\mathbf{B}$ is a unit vector in the direction of the magnetic field and $\mathbf{L}$ is a unit vector in the direction of the camera's view direction, both taken at the tangency plane, for each pixel. In order to obtain the variation in parallel flow along a specific field line, field line tracing is used to find the coordinates in the CIS image where a particular field line of interest intersects the tangency plane. This gives an estimate of the parallel flow at points along the field line spaced approximately half a toroidal turn of the field line.

This experimental flow along a field line, shown in Fig. 8, can then be compared directly with the EMC3-EIRENE simulations in Fig. 5. Qualitatively, smaller diffusion coefficients better match the shape of experimental measurements. The experimental asymmetry may be the result of the top-down asymmetry (as in the modeling), but is additionally impacted by ExB drifts, core plasma rotation, and possibly other MHD effects.

These simulations have been carried out with a single species, with the assumption that impurities will qualitatively follow the behavior of the bulk plasma flow. An examination of parallel impurity transport can verify that this qualitative assumption is true. Taking into account the impurity gradient force, the ion and electron temperature gradient forces, and the frictional force between the impurity ions and the background plasma we find a force balance of[4]:

$$F_{imp} = -\frac{1}{n_{imp}}\frac{dp_{imp}}{ds} + m_{imp}\frac{v_i - v_{imp}}{\tau_s} + \alpha_e\frac{d(kT_e)}{ds} + \beta_i\frac{d(kT_i)}{ds} \quad (8)$$

In this steady state simulation, the forces on the impurity ions will balance, and so the velocity of the impurity ions can be solved for by setting the total force to zero. However, in our Carbon free simulations, electron and ion temperature gradients were minimal outside of the immediate region of the neutral puffing. Naively assuming a constant trace Carbon constant would also eliminate the impurity gradient term and the original ansatz that $v_i = v_{imp}$ is recovered.

To accurately correct for the difference between the bulk ion and impurity velocities will require including

Carbon in the EMC3-EIRENE simulations to determine both the local Carbon density gradients, and the resulting temperature gradients that Carbon emission will cause. However, this more precise treatment of impurity transport is left for future work.

V. CONCLUSION

EMC3-EIRENE modeling was carried out in comparison with MAST experiments with HFS neutral fueling. Good qualitative agreement was found between the flow structures in modeling and the experimentally measured phenomena. In tandem with reduced physics 1-D modeling, the underlying physical mechanism has been identified. The puffed neutrals create a local plasma source, resulting in an increase in plasma pressure, that drives flows away from the fueling perturbation along field lines. Cross field diffusion then damps these flows. Further work will focus on using free modeling parameters (cross field diffusion coefficients, power inputs, etc...) to better match experimental SOL conditions while introducing Carbon impurities into the simulations. These more precise simulations can then be coupled with synthetic diagnostic tools[15] to quantitatively benchmark code results against MAST measurements in preparation for the upcoming MAST-U science campaigns.

ACKNOWLEDGMENTS

This work is funded by the Department of Energy under grant DE- SC0012315 and has been carried out within the framework of the EUROfusion Consortium. It has also received funding from the Euratom research and training program 2014-2018 under grant agreement No 633053 and from the RCUK Energy Program EP/P012450/1. Special thanks to the Culham Centre for Fusion Energy for their hospitality and enthusiasm in enabling this work.

[1] T. E. Evans, R. A. Moyer, K. H. Burrell, M. E. Fenstermacher, I. Joseph, A. W. Leonard, T. H. Osborne, G. D. Porter, M. J. Schaffer, P. B. Snyder, P. R. Thomas, J. G. Watkins, and W. P. West, Nature Physics **2**, 419 (2006).

[2] Y. Liang, H. R. Koslowski, P. R. Thomas, E. Nardon, B. Alper, P. Andrew, Y. Andrew, G. Arnoux, Y. Baranov, M. Bécoulet, M. Beurskens, T. Biewer, M. Bigi, K. Crombe, E. De La Luna, P. De Vries, W. Fundamenski, S. Gerasimov, C. Giroud, M. P. Gryaznevich, N. Hawkes, S. Hotchin, D. Howell, S. Jachmich, V. Kiptily, L. Moreira, V. Parail, S. D. Pinches, E. Rachlew, and O. Zimmermann, Physical Review Letters **98** (2007).

[3] W. Suttrop, T. Eich, J. C. Fuchs, S. Günter, A. Janzer, A. Herrmann, A. Kallenbach, P. T. Lang, T. Lunt, M. Maraschek, R. M. McDermott, A. Mlynek, T. Pütterich, M. Rott, T. Vierle, E. Wolfrum, Q. Yu, I. Zammuto, and H. Zohm, Physical Review Letters **106** (2011).

[4] P. Stangeby, *Plasma Bound. Magn. Fusion Devices* (Institute of Physics Publishing, 2000).

[5] S. A. Silburn, J. R. Harrison, J. Howard, K. J. Gibson, H. Meyer, C. A. Michael, and R. M. Sharples, Review of Scientific Instruments **85** (2014), 10.1063/1.4891165.

[6] J. Howard, Appl. Opt. **41**, 197 (2002).

[7] J. Howard, C. Michael, F. Glass, and A. Cheetham, Rev. Sci. Instrum. **72**, 888 (2001).

[8] Y. Feng, H. Frerichs, M. Kobayashi, and D. Reiter, Plasma Physics and Controlled Fusion **59**, 34006 (2017).

[9] H. Frerichs, O. Schmitz, I. Waters, G. Canal, T. Evans, Y. Feng, and V. Soukhanovskii, Phys. Plasmas **23**, 62517 (2016).

[10] H. Frerichs, O. Schmitz, T. Evans, Y. Feng, and D. Reiter, Phys. Plasmas **22**, 72508 (2015).

[11] D. Harting, D. Reiter, Y. Feng, O. Schmitz, D. Reiser, and H. Frerichs, Plasma Phys. **48**, 197 (2002).

[12] W. Zhang, V. Bobkov, T. Lunt, J.-M. Noterdaeme, D. Coster, R. Bilato, P. Jacquet, D. Brida, Y. Feng, E. Wolfrum, L. Guimarais, and the ASDEX Upgrade Team, Nuclear Fusion **56**, 36007 (2016).

[13] F. Effenberg, Y. Feng, O. Schmitz, H. Frerichs, S. A. Bozhenkov, H. Hölbe, R. König, M. Krychowiak, T. S. Pedersen, D. Reiter, L. Stephey, and W.-X. Team, Nuclear Fusion **57**, 36021 (2017).

[14] Https://github.com/euratom-software/calcam.

[15] H. Frerichs, F. Effenberg, O. Schmitz, C. Biedermann, Y. Feng, M. Jakubowski, R. König, J. Lore, H. Niemann, T. S. Pedersen, L. Stephey, G. A. Wurden, H. Frerichs, F. Effenberg, O. Schmitz, C. Biedermann, Y. Feng, and M. Jakubowski, **441**, 11 (2016).